Integrated Intensity-Based Technique for Coronary Artery Calcium Mass Measurement: A Phantom Study

Dale Black, Xingshuo Xiao, Sabee Molloi

Department of Radiological Sciences, University of California, Irvine,

Irvine, California, 92697, USA

Address for Correspondence:

Sabee Molloi, Ph.D.

Department of Radiological Sciences, Medical Sciences I, B-140

University of California, Irvine, CA 92697

Fax: (949) 824-8115

Telephone: (949) 824-5904

E-mail: symolloi@uci.edu

Abstract

Background

Agatston scoring, the traditional method for measuring coronary artery calcium, is limited in its ability to accurately quantify low-density calcifications, among other things. The inaccuracy of Agatston scoring is likely due partly to the arbitrary thresholding requirement of Agatston scoring.

Purpose

A calcium quantification technique that removes the need for arbitrary thresholding and is more accurate, sensitive, reproducible, and robust is needed. Improvements to calcium scoring will likely improve patient risk stratification and outcome.

Methods

The integrated Hounsfield technique was adapted for calcium scoring (integrated calcium mass). Integrated calcium mass requires no thresholding and includes all calcium information within an image. This study utilized phantom images acquired by G van Praagh et al., with calcium hydroxyapatite (HA) densities in the range of 200-800 $mgHAcm^{-3}$ to measure calcium according to integrated calcium mass and Agatston scoring. The calcium mass was known, which allowed for accuracy, reproducibility, sensitivity, and robustness comparisons between integrated calcium mass and Agatston scoring. Multiple CT vendors (Canon, GE, Philips, Siemens) were used during the image acquisition phase, which provided a more robust comparison between the two calcium scoring techniques. Three calcification inserts of different diameters (1, 3, and 5 mm) and different HA densities (200, 400, and 800 $mgHAcm^{-3}$) were

placed within the phantom. The effect of motion was also analyzed using a dynamic phantom. All dynamic phantom calcium inserts were 5.0 ± 0.1 mm in diameter with a length of 10.0 ± 0.1 mm. The four different densities were 196 ± 3, 380 ± 2, 408 ± 2, and 800 ± 2 mgHAcm^{-3}.

Results

Integrated calcium mass was more accurate than Agatston scoring for stationary scans ($RMSE_{Integrated} = 2.87$, $RMSE_{Agatson} = 4.07$) and motion affected scans ($RMSE_{Integrated} = 9.70$, $RMSE_{Agatson} = 19.98$). On average, integrated calcium mass was more reproducible than Agatston scoring for two of the CT vendors. The percentage of false-negative and false-positive calcium scores were lower for integrated calcium mass (15.00%, 0.00%) than Agatston scoring (28.33%, 6.67%). Integrated calcium mass was more robust to changes in scan parameters than Agatston scoring.

Conclusions

The results of this study indicate that integrated calcium mass is more accurate, reproducible, robust, sensitive, and specific than Agatston scoring on a variety of different CT vendors. The substantial reduction in false-negative scores for integrative calcium scoring is likely to improve risk-stratification for patients undergoing calcium scoring and their potential outcome.

I. Introduction

Coronary artery calcification (CAC) scoring is an important marker of atherosclerosis [1]. Calcium scoring is a technique that utilizes computed tomography (CT) to measure the amount of calcium contained within a patient's coronary arteries. Calcium scoring is a significant predictor of heart disease, the most common cause of death worldwide [2], [3].

Agatston scoring is the most common calcium scoring technique [4]. Agatston scoring is a good predictor of major adverse cardiac events (MACE) [5] but has been shown to characterize a significant number of patients as containing zero-CAC (CAC=0) while still developing MACE [6]. One possible reason for this discrepancy is the intensity-based thresholding that Agatston scoring requires, which makes it hard to detect low-density calcifications below the arbitrary threshold of 130 Hounsfield units. Another possibility is that these patients may have plaques that have not yet calcified [7]. Other techniques like spatially weighted calcium scoring have been proposed as an alternative to Agatston scoring because it does not require any thresholding and improves upon the predictive value of Agatston scoring [8], [9]. Still, spatially weighted calcium scoring is limited in distinguishing low-density CAC from noise since the spatially weighted calcium score always produces a value larger than zero with or without any plaque, and it lacks quantitative meaning due to its arbitrary score without any direct physical correlation.

Agatston scoring produces an arbitrary score but can be turned into a calcium volume score or mass score by calibrating with two known materials, like a water rod and a calcium rod. Calcium

mass scoring techniques within the Agatston regime suffer from many of the same limitations associated with Agatston scoring. A previous study showed that calcium mass scoring results in up to 50% underestimation of calcium mass for large patients [10]–[12]. Urabe et al., showed that patients with a conventional zero-CAC score are more likely to have obstructive stenosis [13]. These discrepancies are likely partially due to the thresholding requirement underlying each technique.

A calcium scoring approach that is more sensitive, specific, accurate, reproducible, and robust would be helpful in the diagnosis and prevention of coronary artery disease. Specifically, measuring undetectable and nearly undetectable calcium levels is challenging with the current approaches, and improving this would help to improve patient risk stratification. Ideally, this calcium scoring method would be quantitative with a direct association to a physical quantity, like mass. The integrated intensity or Hounsfield unit (HU) technique was presented as a novel way to measure coronary artery cross-sectional area [14]. This technique is promising in its ability to calculate area accurately, even past the visible threshold. Until now, this technique was limited to two-dimensional analysis and was not adapted for calcium scoring.

This paper implements a calcium scoring technique in physical phantom computed tomography scans acquired by Praagh et al. [15], based on the integrated HU technique. The integrated calcium mass technique was evaluated against known calcium mass within a standard cardiac calcification phantom and compared to Agatston scoring. This study's calcium scoring algorithms are publicly available at https://github.com/Dale-Black/CalciumScoring.jl.

II. Methods

2.1 – Phantom

This study utilized an anthropomorphic thorax phantom (QRM-Thorax, QRM, Möhrendorf, Germany) with an insert containing calcium (Cardiac Calcification Insert (CCI), QRM, Möhrendorf, Germany). All images were acquired by G van Praagh et al. [15]. The cardiac calcification insert phantom consisted of nine calcification inserts made up of hydroxyapatite (HA). Within the cardiac calcification insert phantom, two calibration rods consisting of water-equivalent material and 200 mgHAcm^{-3} were also present. The calcifications had diameters and lengths of 1.0, 3.0, and 5.0 mm. Three different densities were present in the phantom for each calcification size: 200, 400, and 800 mgHAcm^{-3}. Two different patient sizes, small and large, were included in this analysis by the addition of a fat ring. This fat ring increased the phantom size from 300 × 200 mm to 400 × 300 mm. Figure 1 shows the QRM phantom and cardiac calcification insert phantom diagram. Table 1 shows all the acquisition and reconstruction parameters used in the previously mentioned study.

Segmenting regions of interest is an important step in calcium measurement. For this study, segmentations were done automatically based on previous work by van Praagh et al. [15] and adapted for the Julia programming language [16].

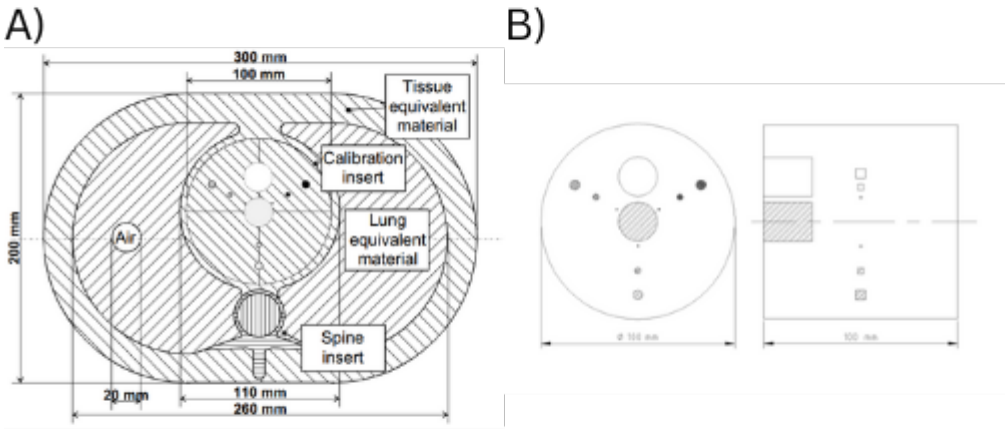

Fig. 1 (A) Shows a sketch of the small QRM-Thorax phantom with the cardiac calcification insert phantom located in the center. (B) Shows an axial and lateral sketch of the cardiac calcification insert phantom.

130

2.1.1 – Motion

A robotic arm (QRM Sim2D, QRM, Möhrendorf, Germany) was also utilized to study the effect of motion on the various calcium scoring techniques. Two artificial coronary artery inserts were used, with each artery consisting of two different density calcifications, resulting in four unique densities. All calcifications were 5.0 ± 0.1 mm in diameter with a length of 10.0 ± 0.1 mm. The four different densities were 196 ± 3, 380 ± 2, 408 ± 2, and 800 ± 2 mgHAcm^{-3}. The arteries were moved at four different constant rates (0-30 mm/s) along the x-axis, comparable to heart rates of 0, <60, 60-75, and >75 bpm. Electrocardiography trigger was used to guarantee that scans were acquired during the linear motion of the arteries. Figure 2 shows a cross-section of a motion-affected artery (Fig. 2B) next to a static artery (Fig. 2A).

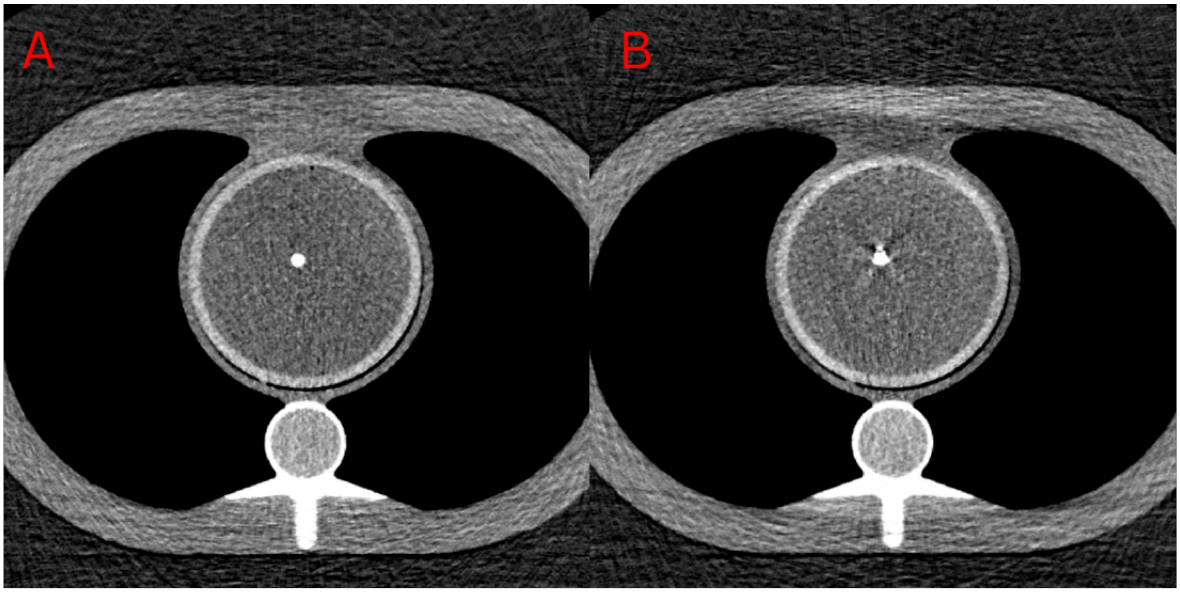

Fig. 2 Shows a cross-section of a static artery (A) next to a cross-section of a motion-affected artery (B). Fig. 2B underwent linear motion at a rate of 30 mm/s, corresponding to a heart rate of >75 bpm. Window: 400, Level: 40.

2.1.2 – Reproducibility

Both phantoms, small and large, were scanned five times with each type of CT vendor to study the reproducibility of each technique. The position of the phantom may have changed between scans, but all other variables remained consistent. We grouped each scan based on vendor (Scanner 1, 2, 3, 4) and then measured the reproducibility, using the first scan as the reference for comparison. Reproducibility measurements were calculated on a vendor-specific basis for the calculated calcium mass of scan 1 compared to the calculated calcium mass of scan 2, scan 3, scan 4, and scan 5 for both the large and small phantoms. The integrated calcium mass and Agatston scoring techniques were then compared to one another by calculating the mean root

mean squared error (RMSE) and deviation (RMSD) values. Equation 1 shows how to calculate RMSE and RMSD. N is the total number of data points, $\hat{y}$ is the calculated calcium masses, and y is either the ground truth calcium masses (RMSE) or the linear regression-based calcium masses (RMSD), which is computed based on the calculated calcium masses.

$$RMS = \sqrt{\frac{\sum |y - \hat{y}|^2}{N}} \quad (1)$$

2.1.3 – Robustness

Various acquisition settings (tube potential, tube current product time, convolution kernel, iterative reconstruction level, field-of-view, and slice thickness) were changed to assess the robustness of the two different calcium scoring techniques. The adjusted settings are consistent with what was previously described [15].

2.2 – Integrated Calcium Mass

As previously reported, the integrated calcium mass technique adapts the integrated Hounsfield technique [17], [18]. The integrated Hounsfield technique accounts for the partial volume effect and avoids arbitrary thresholding by integrating the intensity over an entire region of interest. The total integrated Hounsfield unit is conserved by assuming the partial volume effect only affects a particular voxel and not an entire region.

The cross-sectional area equation (Eq 2), originally proposed by Molloi et al. [14], can be adapted for use in three-dimensional regions (Eq 3) and applied to calcium mass quantification

(Eq 3). Figure 3 shows the cross-section of a simulated coronary plaque with the regions of interest outlined. S_{Obj} is the intensity (HU) of a section of the plaque with pure calcium and no partial volume affected voxels. S_{Bkg} is the measured intensity (HU) of a ring-like section outside the calcified lesion. I is the sum of each voxel intensity (HU) of the lesion that contains all the calcium, including those voxels affected by the partial volume effect. V is the total number of voxels in the entire cross-section multiplied by the voxel size. Equation 4 shows how to convert the volume of the object (V_{Obj}) to mass (M_{Obj}), where $\rho_{S_{Obj}}$ is the density of the calcification, specific to the object intensity (S_{Obj}).

It is impractical to accurately measure the intensity of calcium with no partial volume effect (S_{Obj}) for small calcifications. Therefore, this study utilized a calibration and computed a volume based on an arbitrary S_{Obj}. This volume uses an estimated object signal for S_{Obj} from the calibration linear regression line. Then it converts the volume to mass by multiplying by the density assumed for the calculation of S_{Obj}. In theory, once two calibration points are computed, any input density can be used to estimate S_{Obj} and the corresponding mass calculation. To remain consistent, this study used the calibration rod (200 mgHAcm^{-3}) for one calibration point and background (0 mgHAcm^{-3}) for the other calibration point. Integrating over the entire region of interest should reduce the effect of quantum noise.

$$I = \left[(A - CSA) \times S_{Bkg}\right] + \left[CSA \times S_{Obj}\right]$$

$$CSA = \frac{I - \left(A \times S_{Bkg}\right)}{S_{Obj} - S_{Bkg}} \quad (2)$$

$$I = \left[\left(V - V_{Obj}\right) \times S_{Bkg}\right] + \left[V_{Obj} \times S_{Obj}\right]$$

$$V_{Obj} = \frac{I - \left(V \times S_{Bkg}\right)}{S_{Obj} - S_{Bkg}} \quad (3)$$

$$M_{Obj} = \mathrm{V_{Obj}} \times \rho_{\mathrm{S_{Obj}}} \quad (4)$$

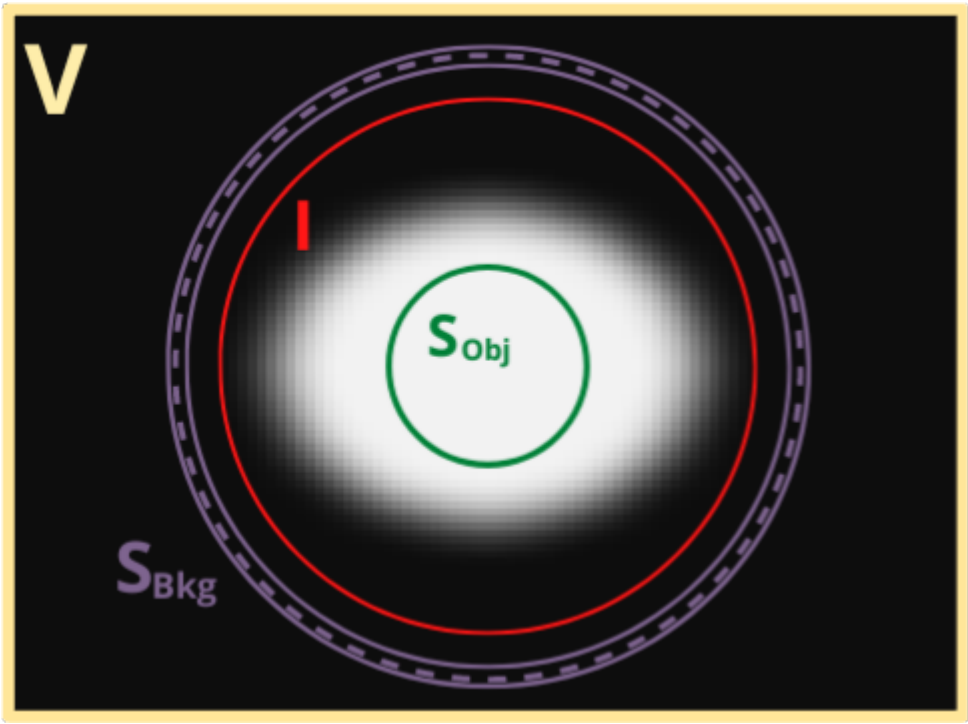

Fig. 3 Shows the cross-section of a simulated vessel lumen. S_{Bkg} and S_{Obj} are regions of pure background and pure calcium, respectively, which are unaffected by the partial volume effect. These are used to calculate I, the integrated intensity of the plaque, which contains pure calcium and voxels affected by the partial volume effect.

2.3 – Statistical Analysis

All calculations were performed using the Julia Programming Language [16]. CalciumScoring.jl, Pluto.jl, Makie.jl, GLM.jl, and MLJ.jl [21]–[25] were used for the calcium scoring and the analysis throughout this study. RMSE and RMSD were calculated for all linear regression measurements.

III. Results

3.1 – Accuracy

Linear regression was performed for integrated calcium mass and Agatston scoring, using the known calcium mass of the inserts as the reference. The images were analyzed in two categories: stationary (no motion) and motion.

3.1.1 – No Motion

Integrated calcium mass (Fig. 4A) was more accurate and precise than Agatston scoring (Fig. 4B), with an RMSE of 2.87 and 4.07, respectively, and an RMSD of 2.69 and 3.31, respectively. The RMSE, RMSD, r-correlation coefficient, and the best-fit line equation for both techniques can be seen in Figure 4.

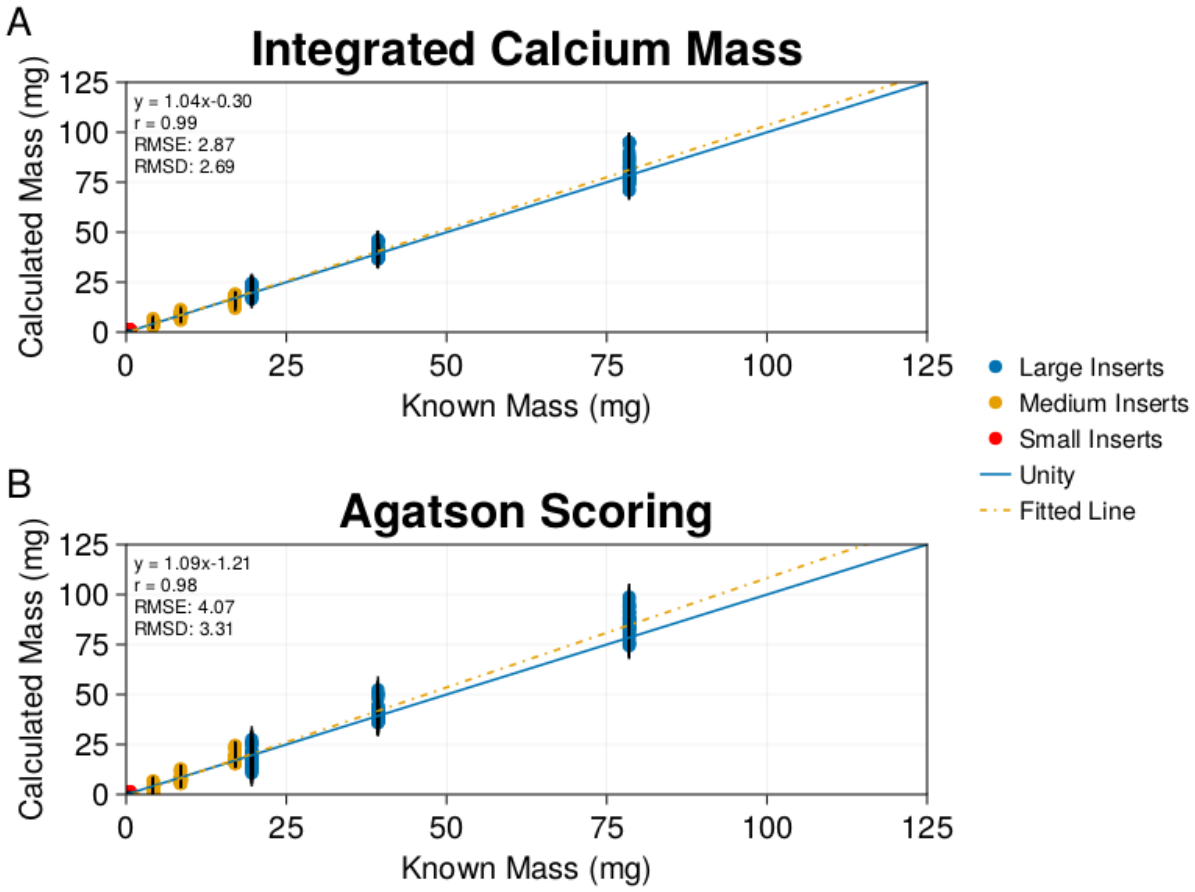

Fig. 4 Shows linear regression analysis of integrated calcium mass (A) and Agatston scoring (B).

The known masses of the calcium inserts were used for the comparison. All inserts were unaffected by motion (stationary).

3.1.2 – Motion

For motion-affected inserts, integrated calcium mass (Fig. 5A) was more accurate and precise than Agatston scoring (Fig. 5B), with an RMSE of 9.70 and 19.98, respectively, and an RMSD of 9.59 and 13.86, respectively. The RMSE, RMSD, r-correlation coefficient, and the best-fit line equation for both techniques can be seen in Figure 5.

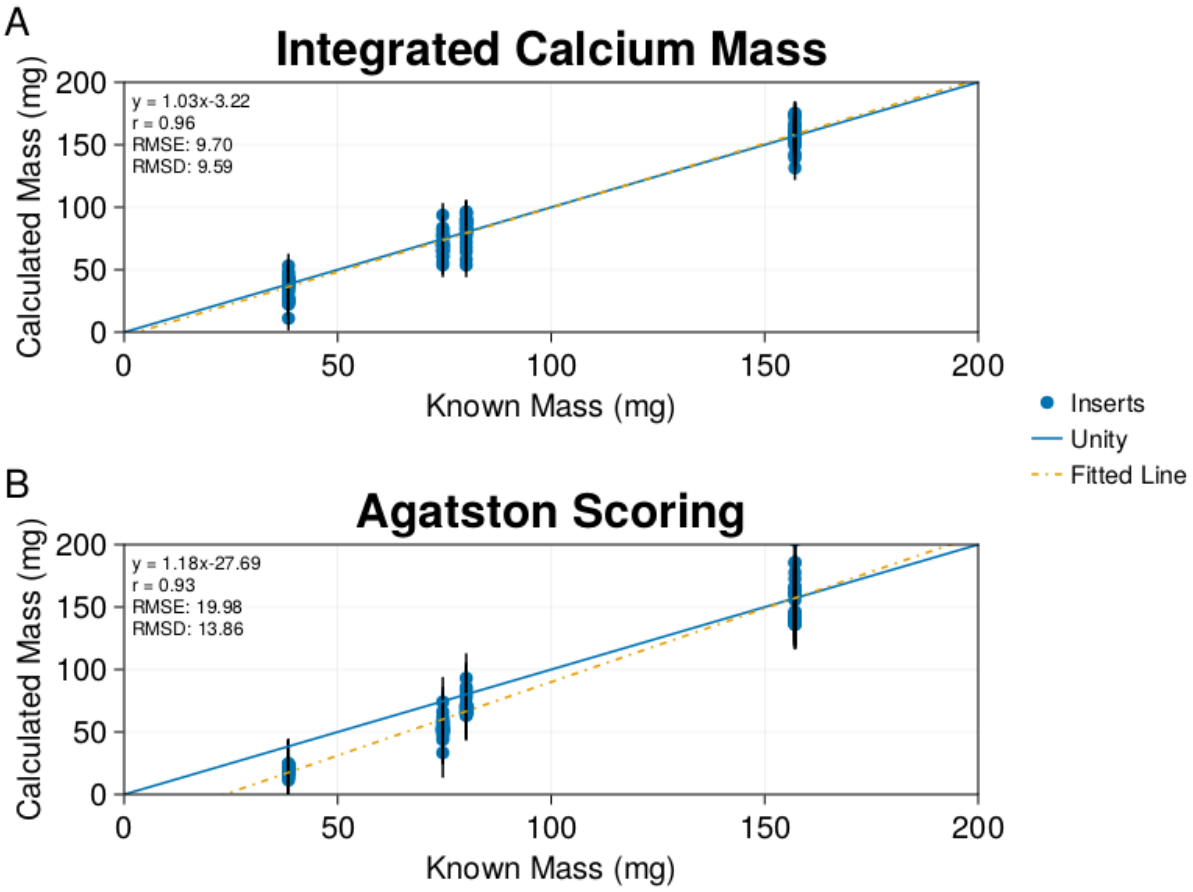

Fig. 5 Shows linear regression analysis of integrated calcium mass (A) and Agatston scoring (B). The known masses of the calcium inserts were used for the comparison. Includes all inserts affected by motion.

3.2 – Reproducibility

Figure 6 shows reproducibility measurements on a vendor-specific basis for the calculated calcium mass of scan 1 compared to the calculated calcium mass of scan 2 using the integrated calcium mass technique. The RMSE was 2.57, 1.92, 1.39, and 2.18 for scanner 1 (Fig. 6A),

scanner 2 (Fig. 6B), scanner 3 (Fig. 6C), and scanner 4 (Fig. 6D), respectively. The RMSD was 0.79, 1.24, 1.23, and 2.09 for scanners 1-4, respectively.

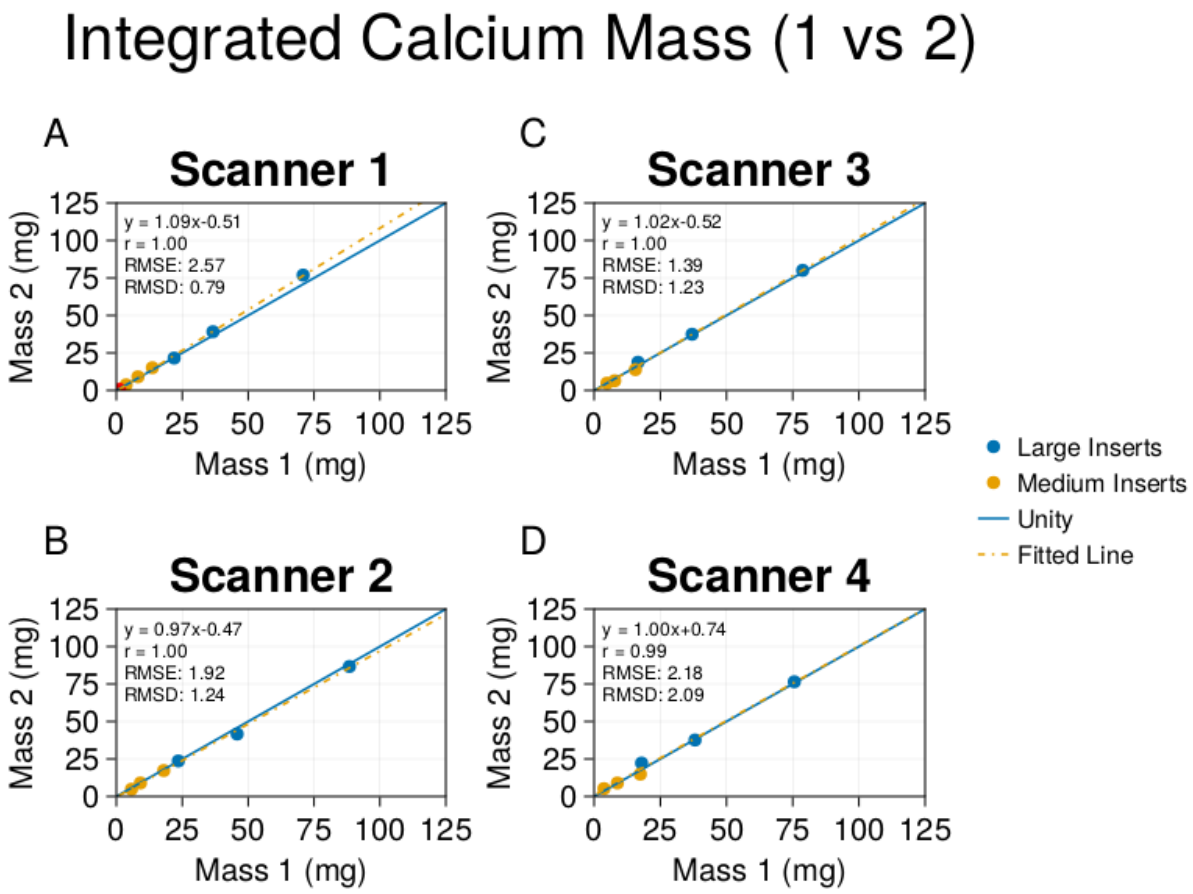

Fig. 6 Shows reproducibility measurements of the integrated calcium mass technique on the large phantoms. The calculated mass for scan 1 was compared against the calculated mass of scan 2. Scanner 1 (A), Scanner 2 (B), Scanner 3 (C), and Scanner 4 (D) were different vendors used to acquire each scan. R correlation, root mean squared error, and root mean squared deviation values are shown within each graph.

Figure 7 shows reproducibility measurements on a vendor-specific basis for the calculated calcium mass of scan 1 compared to the calculated calcium mass of scan 2 using the Agatston

scoring technique. The RMSE was 2.04, 2.59, 0.53, and 0.99 for scanner 1 (Fig. 7A), scanner 2 (Fig. 7B), scanner 3 (Fig. 7C), and scanner 4 (Fig. 7D), respectively. The RMSD was 1.15, 2.04, 0.15, and 0.83 for scanners 1-4, respectively.

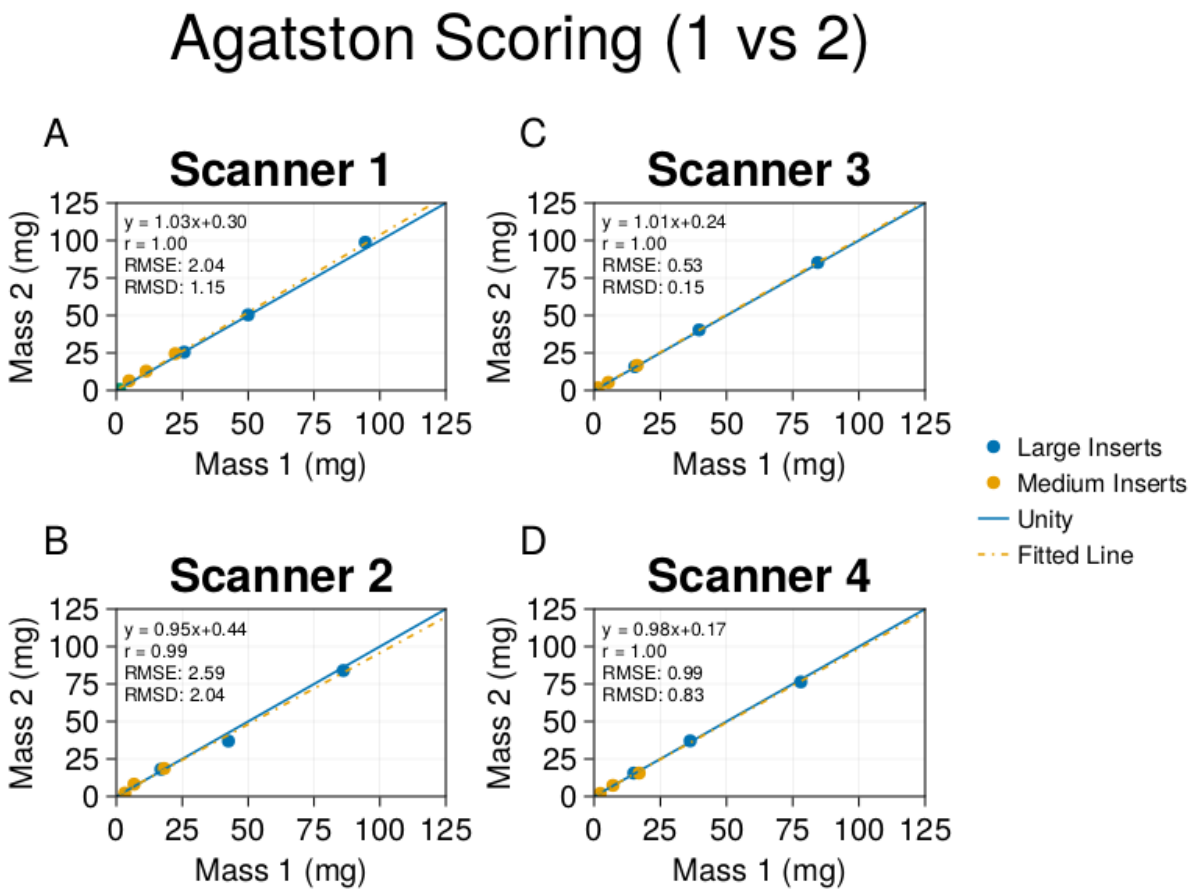

Fig. 7 Shows reproducibility measurements of the Agatston scoring technique on the large phantoms. The calculated mass for scan 1 was compared against the calculated mass of scan 2. Scanner 1 (A), Scanner 2 (B), Scanner 3 (C), and Scanner 4 (D) were different vendors used to acquire each scan. R correlation, root mean squared error, and root mean squared deviation values are shown within each graph.

All ten scans were analyzed (five large phantom scans and five small phantom scans), and RMSE, RMSD, and R-correlation values were computed. Table 2 shows the average RMSE and RMSD values of each vendor. On average, integrated calcium mass had a lower RMSE and RMSD value for Scanners 2-4 but was less reproducible (higher RMSE and RMSD) when using Scanner 1.

3.3 – Sensitivity and Specificity

Agatston scoring produces a false-negative (CAC=0) score whenever a region of interest containing some known calcium returns a CAC score of precisely zero (CAC=0). Integrated calcium mass measures real masses that can be negative or positive, so a false-negative (CAC=0) score was determined to be any mass calculation less than or equal to the mean integrated calcium mass of pure background, plus 1.5 standard deviations. Likewise, a false-positive (CAC>0) score was any mass calculation on pure background that was greater than the mean integrated calcium mass of pure background, 1.5 standard deviations. The additional standard deviation within the threshold helps avoid false-positive (CAC>0) scores for regions with no calcium. Out of 360 total measured calcium regions, integrated calcium mass produced 54 false-negative (CAC=0) scores, while Agatston scoring produced 102 false-negative (CAC=0) scores. Figure 8 shows the percentage of false-negative (CAC=0) and false-positive (CAC>0) scores produced by both techniques. Integrated calcium mass and Agatston scoring resulted in 15.00% and 28.33% false-negative (CAC=0) scores, respectively. Integrated calcium mass and Agatston scoring resulted in 0.00% and 6.67% false-positive (CAC>0) scores, respectively. Table 3 shows the percentage of false-negative and false-positive scores at various thresholds.

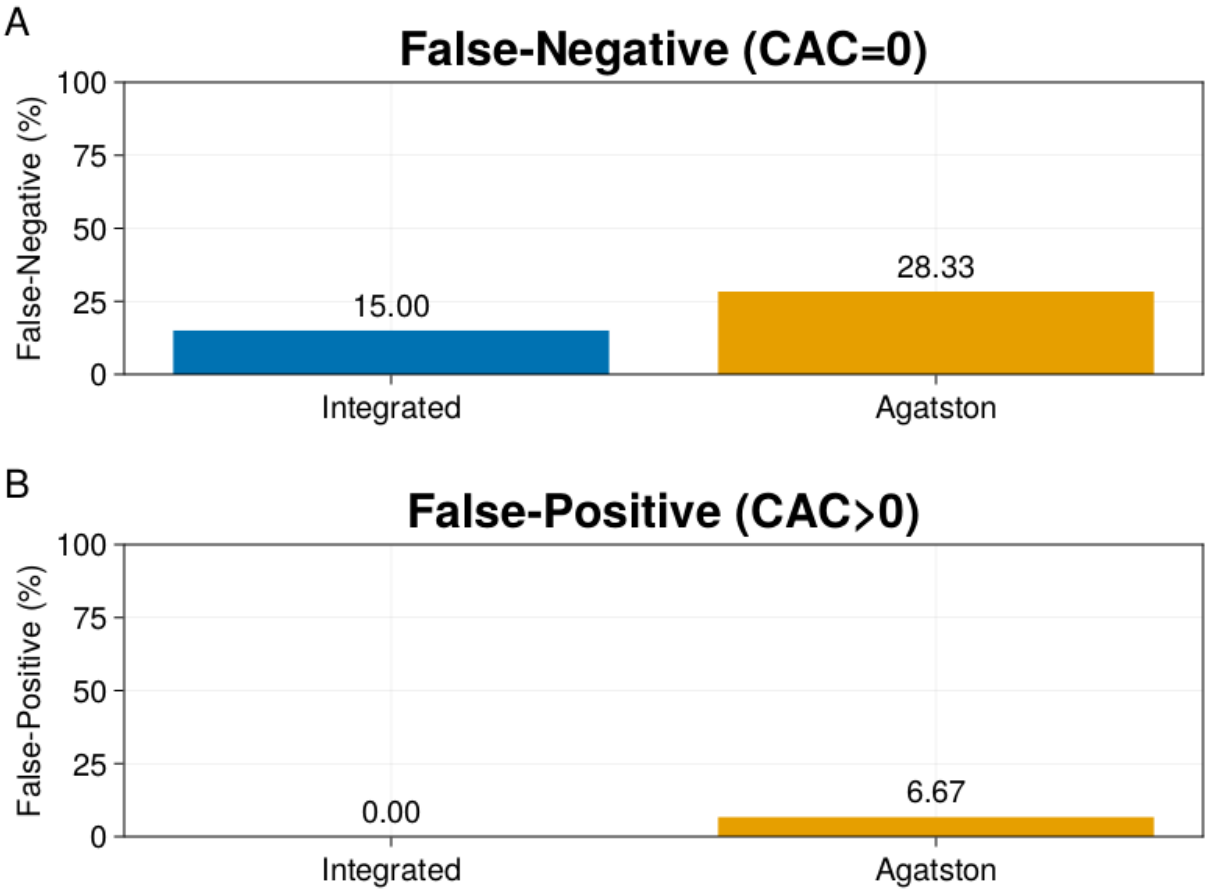

Fig. 8 Shows the percentage of false-negative (CAC=0) scores (A) and false-positive (CAC>0) socres (B), computed by integrated calcium mass (left) and Agatston scoring (right). Integrated calcium mass produced 54 false-negative zero-CAC scores out of 360 total measurements. Agatston scoring produced 102 false-negative zero-CAC scores out of 360 total measurements. Integrated calcium mass produced 0 false-positive (CAC=0) scores out of 120 total measurements. Agatston scoring produced 8 false-negative zero-CAC scores out of 120 total measurements.

Figure 9 shows two different images (Fig. 9A and Fig. 9B) which contain false-negative (CAC=0) scores. Fig. 9A shows an insert (blue arrow) that produced a false-negative (CAC=0) score for both Agatston scoring and integrated calcium mass. Fig. 9B shows a calcium insert (red arrow) that produced a false-negative (CAC=0) score for only Agatston scoring.

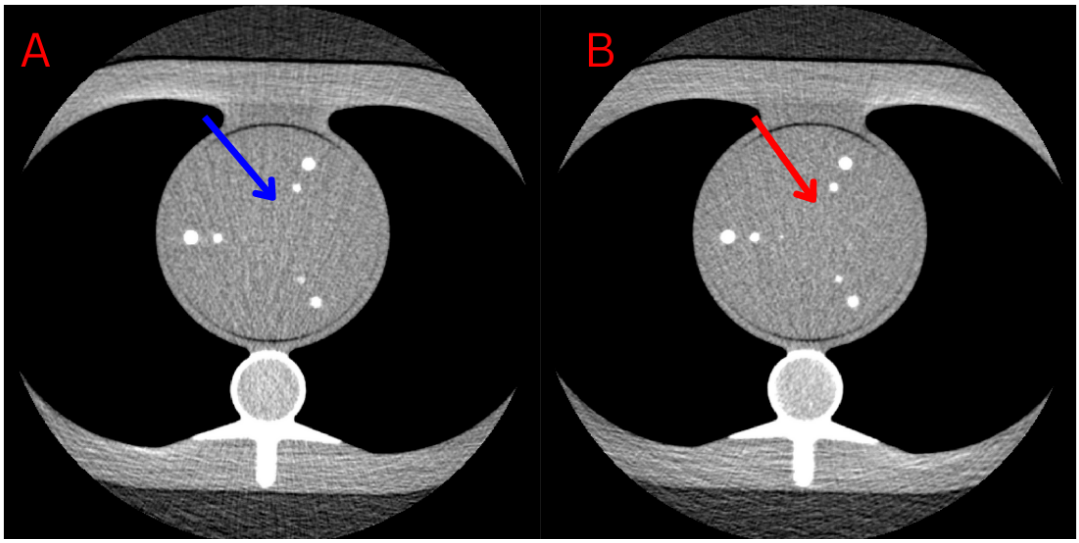

Fig. 9 Shows two different images containing false-negative (CAC=0) scores. Fig. 9A (blue arrow) shows an insert that produced a false-negative (CAC=0) score for both Agatston scoring and integrated calcium mass. Fig. 9B (red arrow) shows a calcium insert that produced a false-negative (CAC=0) score for only Agatston scoring. Window: 400, Level: 40.

3.4 – Robustness

Slice thickness (Fig. 10), tube voltage (Fig. 11), tube current time product, field-of-view, iterative reconstruction level, and convolutional kernel (Table 4) were adjusted to measure the robustness of both calcium scoring techniques. The Siemens SOMATOM Flash (Dynamic)

scanner was used for the robustness study. Each acquisition was acquired under normal conditions, as shown in Table 1, with only one variable (slice thickness, tube voltage, tube current time product, field of view, iterative reconstruction level, and convolutional kernel) subject to change per study. RMSE, RMSD, and R-correlation values were computed for each adjusted parameter and calcium scoring technique. The best-fit line, r-correlation, RMSE, and RMSD values are plotted within each figure (Fig. 10 and 11).

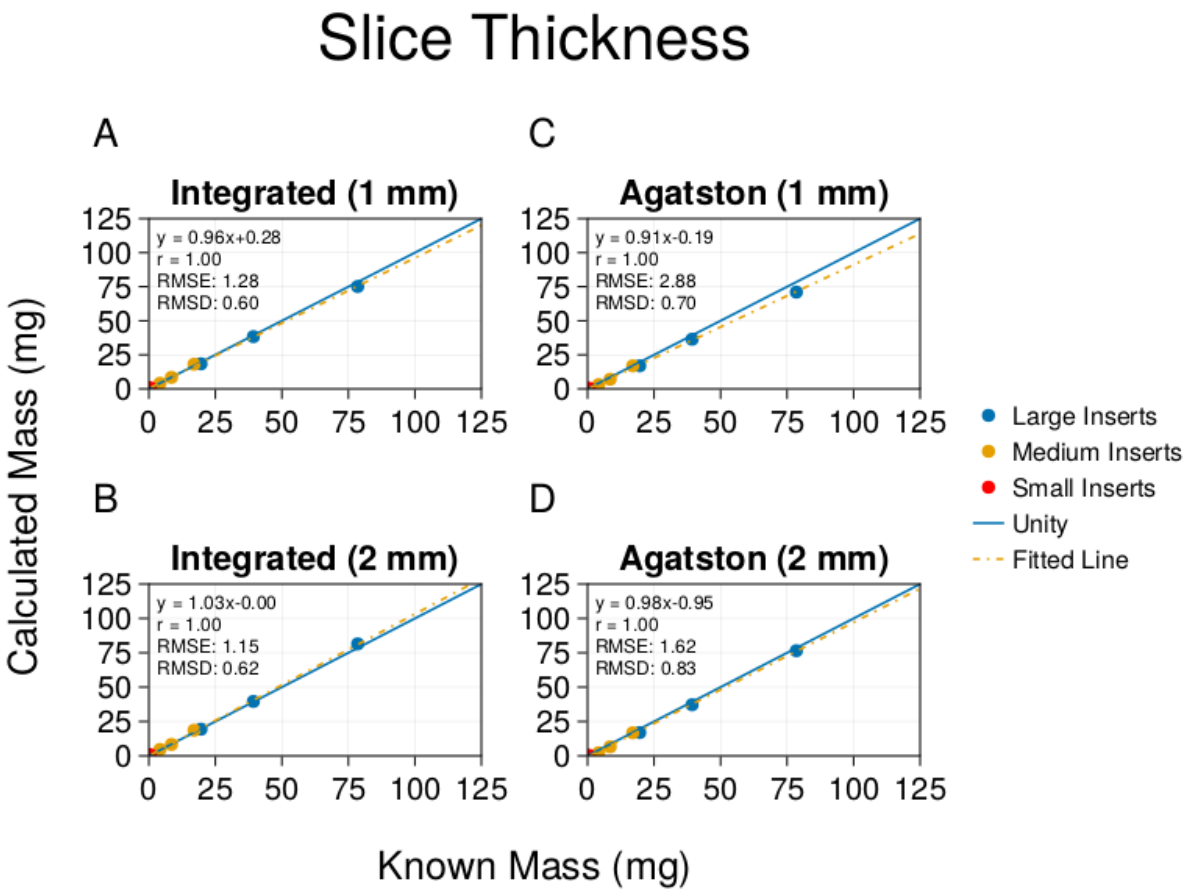

Fig. 10 Shows accuracy measurements of different slice thicknesses for the integrated calcium mass technique (A and B) and the Agatston scoring technique (C and D). A slice thickness of 1

mm (A and C) and 2 mm (B and D) was used. R-correlation, root mean squared error, and root mean squared deviation values are shown within each graph.

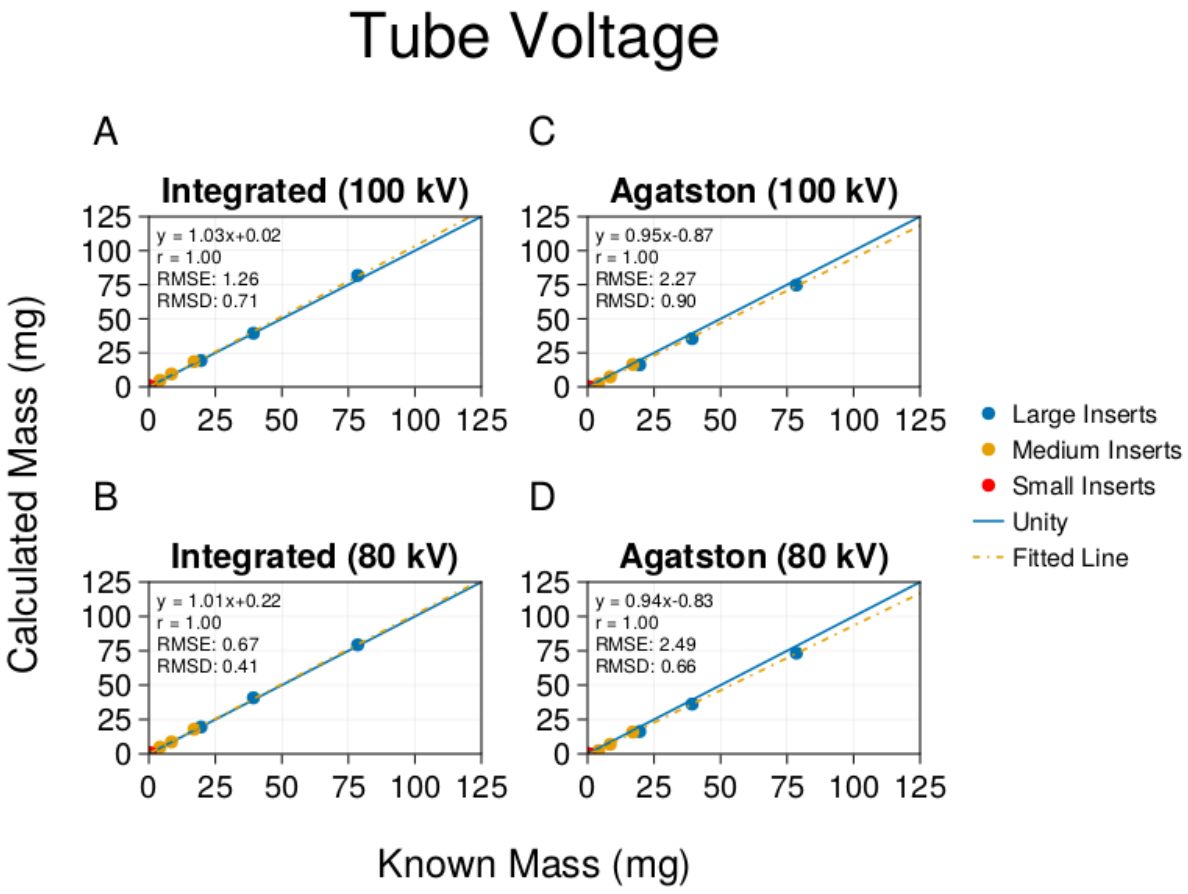

Fig. 11 Shows accuracy measurements of different tube voltages for the integrated calcium mass technique (A and B) and the Agatston scoring technique (C and D). A tube voltage of 100 kV (A and C) and 80 kV (B and D) was used. R-correlation, root mean squared error, and root mean squared deviation values are shown within each graph.

IV. Discussion

Calcium mass was calculated using Agatston scoring and integrated calcium mass on various size and density calcium inserts inside a standard cardiac phantom. Multiple CT vendors were used to acquire the images. The effect of motion was also studied by using a robotic arm attached to the phantom. Lastly, the robustness of each calcium scoring technique was analyzed by changing specific scan parameters, and the calculated mass was compared against the known mass of the calcium inserts.

The results indicate that integrated calcium mass is more accurate than Agatston scoring, with (Fig. 4) and without motion (Fig. 5). On average, integrated calcium mass was more reproducible than Agatston scoring when acquiring images with Scanners 2-4, and less reproducible when utilizing Scanner 1 (Table 2). Integrated calcium mass requires calibration, and this study utilized only two calibration points. Integrated calcium mass might be further improved with more calibration points, especially calibrations near the low-density regime (< 200 $mgHa^{-3}$). This might explain the discrepancy in reproducibility results. Future studies need to be performed, which include multiple calibration rods to help elucidate the importance of calibration on the integrated calcium mass technique's reproducibility.

Previous studies have shown that up to 5% of patients with CAC of zero (CAC=0), according to Agatston scoring, still develop MACE after a follow-up period of 10 years [26]. One question is whether these patients had undetectable calcium due to the thresholding requirements of Agatston scoring or no calcium at all. This study showed that integrated calcium mass resulted

in fewer false-negative (CAC=0) scores than Agatston scoring (Fig. 8). The increased sensitivity of integrated calcium mass could help address the current limitation of patients with false-negative (CAC=0) calcium scores. The fact that the integrated calcium mass does not require manual intervention is important because much of this study is focused on accurately measuring calcium mass for inserts below the threshold of visual detectability. In patients, coronary artery centerline estimates can be extracted in non-contrast CT scans by automatic methods, such as atlas-based approaches [27], [28]. Recently, deep learning has shown promise in automatically segmenting cardiac anatomy and has the potential to accurately segment coronary artery centerlines in non-contrast CT scans, using a supervised learning approach in patient images like the OrCaScore dataset [29]. The coronary artery centerlines can then automatically generate ROIs for calcium mass measurement of coronary artery calcification.

Another limitation of this study is the difference between the calcium inserts in the phantom and calcium contained within the walls of coronary arteries. Unlike the phantom, which contains calcium in the center of an ROI and tissue on the outside, coronary arteries contain hyperattenuating blood within the center of the ROI and hypoattenuating pericoronary adipose tissue surrounding the coronary arteries; assuming an ROI is generated from an ideal centerline extraction in the middle of the coronary artery. Blood has an attenuation range from 17-84 HU, while pericoronary adipose tissue has an attenuation range from -190 to -30 HU [30], [31]. Integrated calcium mass should utilize the entire coronary artery as the region of interest to include all potential calcium in the calculation. With hyperattenuating blood inside these ROIs and hypoattenuating pericoronary adipose tissue located around the ROI, false-positive (CAC>0)

rates would likely increase, relative to this phantom study, due to the inflated integrated intensity (HU) from the blood. Future studies need to be performed on patients to determine optimal mean and standard deviation values that minimize false-negative (CAC=0) and false-positive (CAC>0) scores.

Previous studies show that Agatston scoring consistently underestimates calcium density and volume, with even further underestimation for low-density and motion-affected plaques [32]. Werf et al. indicate that low-density calcifications might fall below the 130 HU threshold because of blurring from motion which artificially reduces the Agatston score [33]. Our study is consistent with these results; we showed that Agatston scoring produced most of the false-negative classifications when calculated on low-density (11.11%) or medium-density (10.6%) calcifications compared to high-density calcifications (6.9%). Future studies are recommended with lower-density calcification inserts (< 200 mgHAcm^3) to understand how integrated calcium mass compares to Agatston mass within the low-density regime. Very high coronary artery calcium density (> 1000 mg/cm^3) is quite rare, and Agatston scoring has already been shown to be a good predictor of cardiovascular disease within this subset of patients [34].

Tzolos et al. showed that Agatston scoring can struggle to detect small calcifications in the coronary arteries of patients due to the threshold requirement of 130 HU and the minimum connected component requirement of 1 mm [35]. Our results are consistent with this study and indicate that the size of the calcium insert is a more important variable in accounting for false-negative Agatston scores than calcium density. The small inserts resulted in 101 false-negative

(CAC=0) scores out of 360 total scores, whereas the medium and large inserts accounted for only one false-negative (CAC=0) score combined. Based on our results, integrated calcium mass overcomes many of these issues associated with Agatston scoring and results in fewer false-negative (CAC=0) and false-positive (CAC>0) scores.

V. Conclusion

The results of this study indicate that integrated calcium mass is more accurate and sensitive than Agatston scoring on various CT vendors. The improved accuracy and sensitivity of integrative calcium scoring is likely to improve risk-stratification for patients undergoing calcium scoring and their potential outcome.

Acknowledgments

The authors would like to thank Drs. Martin Willemink and GD van Praagh for sharing their data for this study. A grant from Canon Medical Systems, USA, partially supported this study.

References

[1] P. Greenland, M. J. Blaha, M. J. Budoff, R. Erbel, and K. E. Watson, "Coronary Calcium Score and Cardiovascular Risk," *J. Am. Coll. Cardiol.*, vol. 72, no. 4, pp. 434–447, Jul. 2018, doi: 10.1016/j.jacc.2018.05.027.

[2] "Predictive Value of Coronary Artery Calcium Score Categories for Coronary Events Versus Strokes: Impact of Sex and Race | Circulation: Cardiovascular Imaging." https://www.ahajournals.org/doi/10.1161/CIRCIMAGING.119.010153 (accessed Jun. 03, 2022).

[3] D. Lloyd-Jones *et al.*, "Executive summary: heart disease and stroke statistics--2010 update: a report from the American Heart Association," *Circulation*, vol. 121, no. 7, pp. 948–954, Feb. 2010, doi: 10.1161/CIRCULATIONAHA.109.192666.

[4] A. S. Agatston, W. R. Janowitz, F. J. Hildner, N. R. Zusmer, M. Viamonte, and R. Detrano, "Quantification of coronary artery calcium using ultrafast computed tomography," *J. Am. Coll. Cardiol.*, vol. 15, no. 4, pp. 827–832, Mar. 1990, doi: 10.1016/0735-1097(90)90282-T.

[5] M. S. Lo-Kioeng-Shioe *et al.*, "Coronary Calcium Characteristics as Predictors of Major Adverse Cardiac Events in Symptomatic Patients: Insights From the CORE320 Multinational Study," *J. Am. Heart Assoc.*, vol. 8, no. 6, p. e007201, Mar. 2019, doi: 10.1161/JAHA.117.007201.

[6] D. E. Bild *et al.*, "Multi-Ethnic Study of Atherosclerosis: Objectives and Design," *Am. J. Epidemiol.*, vol. 156, no. 9, pp. 871–881, Nov. 2002, doi: 10.1093/aje/kwf113.

[7] M. B. Mortensen *et al.*, "Association of Age With the Diagnostic Value of Coronary Artery Calcium Score for Ruling Out Coronary Stenosis in Symptomatic Patients," *JAMA Cardiol.*, vol. 7, no. 1, pp. 36–44, Jan. 2022, doi: 10.1001/jamacardio.2021.4406.

[8] S. Shea *et al.*, "Spatially Weighted Coronary Artery Calcium Score and Coronary Heart Disease Events in the Multi-Ethnic Study of Atherosclerosis," *Circ. Cardiovasc. Imaging*, vol. 14, no. 1, p. e011981, Jan. 2021, doi: 10.1161/CIRCIMAGING.120.011981.

[9] C. J. Liang, M. J. Budoff, J. D. Kaufman, R. A. Kronmal, and E. R. Brown, "An alternative method for quantifying coronary artery calcification: the multi-ethnic study of atherosclerosis (MESA)," *BMC Med. Imaging*, vol. 12, p. 14, Jul. 2012, doi: 10.1186/1471-2342-12-14.

[10] M. J. Willemink *et al.*, "Coronary Artery Calcification Scoring with State-of-the-Art CT Scanners from Different Vendors Has Substantial Effect on Risk Classification," *Radiology*, vol. 273, no. 3, pp. 695–702, Dec. 2014, doi: 10.1148/radiol.14140066.

[11] M. J. Blaha, M. B. Mortensen, S. Kianoush, R. Tota-Maharaj, and M. Cainzos-Achirica, "Coronary Artery Calcium Scoring: Is It Time for a Change in Methodology?," *JACC Cardiovasc. Imaging*, vol. 10, no. 8, pp. 923–937, Aug. 2017, doi: 10.1016/j.jcmg.2017.05.007.

[12] "Coronary calcium scores are systematically underestimated at a large chest size: A multivendor phantom study - ClinicalKey." https://www.clinicalkey.com/#!/content/playContent/1-s2.0-S1934592515001070?returnurl=null&referrer=null (accessed Nov. 11, 2022).

[13] Y. Urabe *et al.*, "Identifying Small Coronary Calcification in Non-Contrast 0.5-mm Slice Reconstruction to Diagnose Coronary Artery Disease in Patients with a Conventional Zero Coronary Artery Calcium Score," *J. Atheroscler. Thromb.*, vol. 23, no. 12, pp. 1324–1333, Dec. 2016, doi: 10.5551/jat.35808.

[14] S. Molloi, T. Johnson, H. Ding, and J. Lipinski, "Accurate quantification of vessel cross-sectional area using CT angiography: a simulation study," *Int. J. Cardiovasc. Imaging*, vol. 33, Mar. 2017, doi: 10.1007/s10554-016-1007-9.

[15] G. D. Praagh *et al.*, "Fully automated quantification method (FQM) of coronary calcium in an anthropomorphic phantom," *Med. Phys.*, vol. 48, no. 7, pp. 3730–3740, Jul. 2021, doi: 10.1002/mp.14912.

[16] J. Bezanson, A. Edelman, S. Karpinski, and V. B. Shah, "Julia: A Fresh Approach to Numerical Computing," *SIAM Rev.*, vol. 59, no. 1, pp. 65–98, Jan. 2017, doi: 10.1137/141000671.

[17] D. Black, S. Molloi, X. Xiao, S. Shen, and S. Nie, "Accurate and Robust Quantification of Calcium Mass in Coronary Artery Calcium Using the Integrated Hounsfield Technique," presented at the AAPM 2022, 64th Annual Meeting and Exhibition, Jul. 2022. Accessed: Aug. 08, 2022. [Online]. Available: https://w4.aapm.org/meetings/2022AM/programInfo/programAbs.php?sid=10792&aid=66792

[18] D. Black, X. Xiao, Y. Shen, S. Nie, and S. Molloi, "498 Quantification Of Calcium Mass For Cases With Near Zero Coronary Artery Calcium Score," *J. Cardiovasc. Comput. Tomogr.*, vol. 16, no. 4, p. S47, Jul. 2022, doi: 10.1016/j.jcct.2022.06.109.

[19] J. M. Boone, T. R. Fewell, and R. J. Jennings, "Molybdenum, rhodium, and tungsten anode spectral models using interpolating polynomials with application to mammography," *Med. Phys.*, vol. 24, no. 12, pp. 1863–1874, Dec. 1997, doi: 10.1118/1.598100.

[20] J. M. Boone and A. E. Chavez, "Comparison of x-ray cross sections for diagnostic and therapeutic medical physics," *Med. Phys.*, vol. 23, no. 12, pp. 1997–2005, Dec. 1996, doi: 10.1118/1.597899.

[21] "Dale-Black/CalciumScoring.jl: Initial Release | Zenodo." https://zenodo.org/record/6903873 (accessed Aug. 11, 2022).

[22] D. Bates *et al.*, "JuliaStats/GLM.jl: v1.8.0." Zenodo, May 25, 2022. doi: 10.5281/zenodo.6580436.

[23] S. Danisch and J. Krumbiegel, "Makie.jl: Flexible high-performance data visualization for Julia," *J. Open Source Softw.*, vol. 6, no. 65, p. 3349, Sep. 2021, doi: 10.21105/joss.03349.

[24] F. van der Plas *et al.*, "fonsp/Pluto.jl: v0.19.11." Zenodo, Jul. 27, 2022. doi: 10.5281/zenodo.6916713.

[25] "DataFrames.jl/index.md at main · JuliaData/DataFrames.jl," *GitHub*. https://github.com/JuliaData/DataFrames.jl (accessed Jun. 01, 2022).

[26] M. J. Budoff *et al.*, "Ten-year association of coronary artery calcium with atherosclerotic cardiovascular disease (ASCVD) events: the multi-ethnic study of atherosclerosis (MESA)," *Eur. Heart J.*, vol. 39, no. 25, pp. 2401–2408, Jul. 2018, doi: 10.1093/eurheartj/ehy217.

[27] J. M. Wolterink, T. Leiner, R. A. P. Takx, M. A. Viergever, and I. Išgum, "Automatic Coronary Calcium Scoring in Non-Contrast-Enhanced ECG-Triggered Cardiac CT With

Ambiguity Detection," *IEEE Trans. Med. Imaging*, vol. 34, no. 9, pp. 1867–1878, Sep. 2015, doi: 10.1109/TMI.2015.2412651.

[28] R. Shahzad *et al.*, "Vessel Specific Coronary Artery Calcium Scoring," *Acad. Radiol.*, vol. 20, no. 1, pp. 1–9, Jan. 2013, doi: 10.1016/j.acra.2012.07.018.

[29] J. M. Wolterink *et al.*, "An evaluation of automatic coronary artery calcium scoring methods with cardiac CT using the orCaScore framework," *Med. Phys.*, vol. 43, no. 5, pp. 2361–2373, 2016, doi: 10.1118/1.4945696.

[30] S. D. Qanadli, A.-M. Jouannic, J. Dehmeshki, and T.-L. Lu, "CT Attenuation Values of Blood and Myocardium: Rationale for Accurate Coronary Artery Calcifications Detection with Multi-Detector CT," *PLoS ONE*, vol. 10, no. 4, p. e0124175, Apr. 2015, doi: 10.1371/journal.pone.0124175.

[31] L. V. Klüner, E. K. Oikonomou, and C. Antoniades, "Assessing Cardiovascular Risk by Using the Fat Attenuation Index in Coronary CT Angiography," *Radiol. Cardiothorac. Imaging*, vol. 3, no. 1, p. e200563, Feb. 2021, doi: 10.1148/ryct.2021200563.

[32] J. Šprem *et al.*, "Coronary calcium scoring with partial volume correction in anthropomorphic thorax phantom and screening chest CT images," *PLOS ONE*, vol. 13, no. 12, p. e0209318, Dec. 2018, doi: 10.1371/journal.pone.0209318.

[33] N. R. van der Werf, M. J. Willemink, T. P. Willems, R. Vliegenthart, M. J. W. Greuter, and T. Leiner, "Influence of heart rate on coronary calcium scores: a multi-manufacturer phantom study," *Int. J. Cardiovasc. Imaging*, vol. 34, no. 6, pp. 959–966, Jun. 2018, doi: 10.1007/s10554-017-1293-x.

[34] A. W. Peng *et al.*, "Very High Coronary Artery Calcium (≥1000) and Association With Cardiovascular Disease Events, Non–Cardiovascular Disease Outcomes, and Mortality," *Circulation*, vol. 143, no. 16, pp. 1571–1583, Apr. 2021, doi: 10.1161/CIRCULATIONAHA.120.050545.

[35] E. Tzolos *et al.*, "Detection of small coronary calcifications in patients with Agatston coronary artery calcium score of zero," *J. Cardiovasc. Comput. Tomogr.*, vol. 16, no. 2, pp. 150–154, Mar. 2022, doi: 10.1016/j.jcct.2021.10.004.